Scripta Materialia 114 (2016) 74–78

Contents lists available at ScienceDirect

Scripta Materialia

journal homepage: www.elsevier.com/locate/scriptamat

Regular Article

Anisotropic swelling and microcracking of neutron irradiated Ti_3AlC_2–$Ti_5Al_2C_3$ materials

Caen Ang [a,*], Chinthaka Silva [a], Chunghao Shih [a], Takaaki Koyanagi [a], Yutai Katoh [a], Steven J. Zinkle [a,b]

[a] Oak Ridge National Laboratory, P.O. Box 2008, Oak Ridge, TN 37831, USA
[b] University of Tennessee, Knoxville, TN, USA

ARTICLE INFO

Article history:
Received 23 September 2015
Received in revised form 1 November 2015
Accepted 9 November 2015
Available online 17 December 2015

Keywords:
Anisotropic swelling
Neutron irradiation
MAX phase
Microcracking
Lattice parameter

ABSTRACT

$M_{n+1}AX_n$ (MAX) phase materials based on Ti–Al–C have been irradiated at 400 °C (673 K) with fission neutrons to a fluence of 2×10^{25} n/m^2 (E > 0.1 MeV), corresponding to ~2 displacements per atom (dpa). We report preliminary results of microcracking in the Al-containing MAX phase, which contained the phases Ti_3AlC_2 and $Ti_5Al_2C_3$. Equibiaxial ring-on-ring tests of irradiated coupons showed that samples retained 10% of pre-irradiated strength. Volumetric swelling of up to 4% was observed. Phase analysis and microscopy suggest that anisotropic lattice parameter swelling caused microcracking. Variants of titanium aluminum carbide may be unsuitable materials for irradiation at light water reactor-relevant temperatures.

Ti_3AlC_2 belongs to a class of materials known as MAX ($M_{n+1}AX_n$) phases, where M is an early transition metal, A is an A-group element and X is either C or N [1]. The lamellar "A-layer" metal atoms alternating with "MX" ceramic unit cells give a combination of metal and ceramic properties [2,3]. For radiation resistance, the lamellae represent nanoscale interfaces that may function as natural sinks for mitigating defect accumulation responsible for degradation of materials under irradiation [4]. They are proposed as candidate materials for fiber-reinforced composites and environmental barrier coatings in light water reactors.

Crystal structure and phase changes from ion irradiation have been explored for both Al- and Si-containing MAX phases. Room temperature ion irradiation established that Ti_3AlC_2 is resistant to amorphization by 50 and 500 keV He ions; lattice periodicity was disturbed by 20 displacements per atom (dpa) but no amorphization was reported after 31 and 52 dpa [5–7]. Radiation-induced decomposition of $Ti_3(Al,Si)C_2$ to TiC has been reported by several authors based on XRD analysis [6,8]. When irradiated by neutrons at ~360 °C, Tallman et al. reported extensive decomposition of Ti_3AlC_2, with an increase of 48 wt.% TiC after 0.1 dpa accompanied by ~1.8% (Δc/c) c-axis elongation; the equivalent Ti_3SiC_2-CG (coarse grain) material showed increased TiC content of 2.75 wt.% with a corresponding ~0.9% c-axis elongation [9]. The Ti_2AlC material appeared to be more thermodynamically stable under irradiation, with an increase of 2.5 wt.% TiC and a c-axis elongation of ~1.68% [9]. For some reason, most ion irradiations on Ti_3AlC_2 have not reported significant lattice parameter changes after irradiation from 10 to 52 dpa [5,7,10,11]. At an irradiation temperature (T_{irr}) of 400 °C using 5.8 MeV Ni ions, Clark et al. recently reported Δc/c expansions at 10 and 30 dpa [12]. Here we summarize post-irradiation characterization of samples after T_{irr} ~ 400 °C, at ~2 dpa on predominantly Ti_3AlC_2 materials. Partial quantitative phase analysis, crystallite size, microstrain and lattice parameters were obtained. Volumetric swelling and mechanical properties are reported.

Commercially available MAX phase materials (3-ONE-2, LLC (Willow Grove, PA)) were cold isostatically pressed ternary powders and pressurelessly sintered by the manufacturer. Machined disc coupons (6 × 6 × 0.5 mm) and multi-purpose beam (25 × 2 × 1.5 mm) specimens were inserted into a holder of fast-neutron resistant V–4Ti–4Cr alloy and sealed in helium atmosphere [13]. Neutron irradiation was conducted at the High-Flux Isotope Reactor (HFIR) at Oak Ridge National Laboratory (ORNL) to a fast neutron fluence of 2×10^{25} n/m^2 (E > 0.1 MeV), producing an estimated atomic displacement damage of ~2 dpa. The irradiation temperature (T_{irr}) was determined by SiC temperature monitors (TMs) inserted in the capsules [14,15,16]. The exterior SiC TMs reached an irradiation temperature of 370 °C. Thermal contour maps (not shown) yielded specimen temperatures between 401 °C to 460 °C. XRD patterns of both as-received and post-irradiated materials were acquired using Cu Kα (40 kV, 40 mA) radiation using a Scintag X-ray Diffractometer. Samples were mounted on a zero-background (SiO_2 Optical Grade from MTIXTI) mount. An internal Si SRM640b standard was used for lattice parameter refinements. Full profile fits of the XRD patterns were performed using GSAS [17]. Crystallite size and strain were calculated by Williamson–Hall method. Discs were machined and polished to a 1 μm finish with a series of

* Corresponding author.

http://dx.doi.org/10.1016/j.scriptamat.2015.11.008
1359-6462/

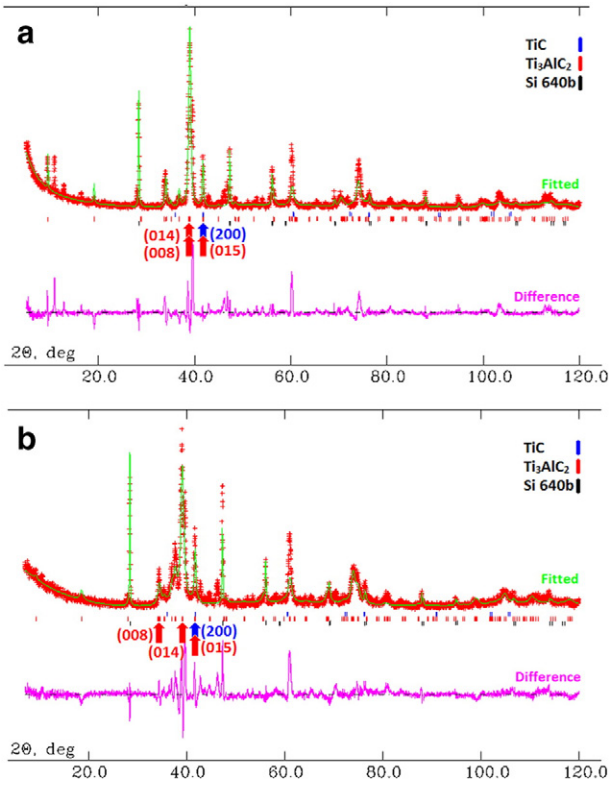

Fig. 1. XRD patterns of Ti–Al–C material showing that the (015) Ti_3AlC_2 peak overlaps with the TiC (200) peak in both (a) as-machined and (b) post-irradiation at 406(25)°C. The shift in the identified (008) peak for Ti_3AlC_2 is also shown.

diamond polishing pastes. Scanning Electron Microscopy was conducted with a JEOL 6500F SEM equipped with an EDAX Hikari camera. Volumetric swelling was measured from the volume of the exact 25 mm modulus bar inserted into the capsule. Length was measured at 90° intervals around the edges and the average value taken to be equal the length of the specimen. Four measurements were taken of the height and width. Precision of all measurements was better than ±3 μm. Equibiaxial flexural strength measured according to ASTM C1499 was conducted on a minimum of 3 specimens [18].

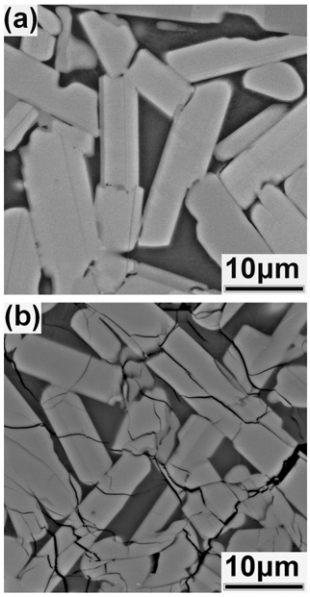

Fig. 2. Backscattered electron images of Ti–Al–C before (a) and after (b) irradiation.

Table 1
Result of quantitative phase analysis of Ti–Al–C material. Values show wt% phase composition.

Phase	Ti_3AlC_2	TiC	Ti_2AlC	$Ti_5Al_2C_3$	Ti_5Al_{11}
Space group	P 63/m m c	F m − 3 m	P 63/m m c	P 63/m m c	
Relative wt.% of phases					
Scintag Cu Kα	76.6	20.2	Not fitted	Not fitted	3.2
Scintag T_{irr} 406(25)°C	71.9	28.1	Not fitted	Not fitted	

The XRD pattern for Ti–Al–C material is shown in Fig. 1 for as-machined and neutron irradiated samples. The reference phases that were able to be indexed are shown below the two patterns. Fig. 1(a) shows unirradiated material. The region around 37–40° indexes with several MAX phase materials of Ti_2AlC and $Ti_5Al_2C_3$, although most of the material appears to be the Ti_3AlC_2 phase. The Si standard is marked in both patterns. In Fig. 1(b), considerable broadening of the diffraction peaks following neutron irradiation is evident along with the appearance of new peaks either due to reflections that are no longer extinct after neutron irradiation, or substantial peak shift. The key features to note are the position of the (015) peak of the Ti_3AlC_2 reflection which overlaps with the phase identified as TiC (200) in both (a) and (b), and in Fig. 2(b), the substantial shift of the (008) Ti_3AlC_2 peak after irradiation.

The quantitative phase analysis (QPA) of Ti–Al–C material (Table 1) should be used with caution. Ti_2AlC and Ti_3AlC_2 possess identical space groups and the software was not designed for analysis of highly defected lattices. As crystallographic data was crucial to interpretation of the microstructural changes, a compromise was obtained by fitting *only* the Ti_3AlC_2 peaks, so that radiation-induced changes in lattice parameters could be obtained.

It is safe to state that under irradiation, the relative quantity of Ti_3AlC_2 (which likely includes convolutions of $Ti_5Al_2C_3$ + Ti_3AlC_2) is reduced by at least 4.7 wt.% due to reduced integrated intensity. There is an increase in either Ti_2AlC or TiC content. This increase was difficult to identify because the major peak for TiC (200) overlaps to Ti_3AlC_2 (015) and the refinement for Ti_3AlC_2 probably included $Ti_5Al_2C_3$ (which includes the Ti_2AlC subcell). It is worth noting that the high angle peaks for TiC were not found beyond 60°, notably the (311) and (420) peaks, only a possible (200) match. Thus we cannot definitively report Ti_3AlC_2 decomposition to TiC by XRD. The absence of high angle peaks could also indicate highly oriented Ti and C defect clusters, since the basic unit of TiC is a <200> Ti–C bond. Note that SEM imaging seen later shows that the volume of intermetallic appears unchanged after irradiation.

Lattice parameter (LP), crystallite size and microstrain values for the phase fitted to Ti_3AlC_2 is shown in Table 2 (parenthesis indicate ± error margin). After irradiation to ~2 dpa at 406(25)°C, a change in the MAX phase lattice parameter occurs. This calculates to 3.1% c-axis change (Δc/c) and −1.0% a-axis change (Δa/a). For comparison, Δc/c of 1.8% and Δa/a of −0.64% was reported for Ti_3AlC_2 after 0.1 dpa at ~360(20)°C [9].

After irradiation, the crystallite size substantially decreased. Interestingly, microstrain data indicated that the Ti–Al–C materials were affected by the pressureless sintering or machining, perhaps due to

Table 2
Lattice parameters, crystallite size and microstrain of Ti–Al–C phases (fitted as Ti_3AlC_2). (Parenthesis indicate ± error margin).

	Pre-irradiation	Post-irradiation
	Ti_3AlC_2	Ti_3AlC_2
LP a (A)	3.0651(1);	3.0345(2);
LP c (C)	18.5307(2)	19.1135(29)
Crystallite size (nm)	794.5	13.3
Microstrain (%)	0.4874	0.0239

Table 3
Room temperature ring-on-ring fracture strength after irradiation at 2 dpa. Sf denotes normal average for equibiaxial flexural strength with one standard deviation in parentheses.

Material/ID	Irradiation temperature (°C)	σ_f (MPa)
Ti–Al–C (31 tests)	As machined	307.8 (15.8)
Ti–Al–C (3 tests)	416(25)°C	28 (5.3)

thermal mismatch between intermetallics and ceramic phases. This suggested that the material annealed or underwent creep in the irradiation capsule.

Fig. 2(a) shows the morphology of the as-received material. A Back-Scattered Electron (BSE) detector was used and shows limited phase identification. Ti–Al–C grains can clearly be seen by their anisotropic appearance and are up to 40 μm in length. The intermetallic phase is observed as the darker regions, but was not quantified in XRD due to aforementioned challenges. Channeling contrast in some of the grains reveals the c-axis stacking contrast, which is presumed to be the different MAX phases (e.g. one grain may be Ti_3AlC_2 alongside $Ti_5Al_2C_3$). Fig. 2(b) shows the neutron irradiated Ti–Al–C material. Extensive transgranular and cracking through the material was observed.

The volumetric swelling from irradiation ($\Delta V_{irr}/V_{irr}$) of Ti–Al–C was 4.0%. The swelling clearly includes a volume expansion occupied by microcracks observed in Fig. 2(b). It is possible that a substantial intragranular formation of TiC also causes the gross volume change. Regardless, Fig. 2(b) does not promise a load-bearing microstructure, and this is demonstrated by equibiaxial ring-on-ring testing on multipurpose square discs at room temperature. Table 3 shows the as-received strength of 308(16) MPa (31 specimens) and post-irradiation value of 28(5) MPa.

It appears that microcracking resulted in a substantial loss of strength. Similar effects associated with anisotropic swelling have been observed in neutron irradiated ceramics with hexagonal close packed (HCP) crystal structures such as BeO, AlN and Al_2O_3 [19–21]. These studies monitored Δc/c and Δa/a lattice parameter (LP) values and attributed the microcracking resulting in a loss of strength to anisotropic irradiation strains in the HCP crystallites. Fig. 3 shows the published data on Ti_3AlC_2 anisotropic lattice swelling on the same plot of Δc/c and Δa/a. The values were calculated from published XRD lattice parameters or commentary. Projectile energy, ion species, author, T_{irr}, and other analysis technique (GXRD, TEM) are shown.

In Fig. 3, the data from room temperature ("25 °C") ion irradiations by Huang, Wang and Yang show negligible values of Δc/c and Δa/a [5,10,11]. The maximum reported c-axis expansion was 0.09%, however, values from 5.6 to 6.29% were obtained when Δc/c was fitted to a modified β-Ti_3AlC_2, marked as β in Fig. 3 [11]. This is discussed later. The high temperature data (in solid markers) from 400 °C to 700 °C shows measurable c-axis expansion and a-axis shrinkage. Neutron data for T_{irr} ~ 400 °C yields Δc/c of 1.8% at 0.1 dpa and 2.7% at 2 dpa and the corresponding Δa/a values are −0.63% and −1.0% respectively [9]. Ion irradiation by Clark et al. at T_{irr} ~ 400 °C showed Δc/c of 1% at 10 dpa, and Δa/a of −0.11% [12]. Both ion and neutron data at T_{irr} ~ 700 °C show reduced Δc/c and Δa/a compared to ~400 °C; Clark et al. showed 0.3% Δc/c and −0.11% Δa/a for ion irradiation at 10 dpa, and Tallman et al. showed no changes at 695 °C after 0.1 dpa [9,11]. Fig. 3 shows that the magnitude of Δc/c and Δa/a is consistent; it indicates that damage mechanisms affecting Δc/c and Δa/a are similar for ion and neutron irradiation, and correspond to an anisotropic lattice swelling. There is some conflict between neutron and ion irradiation data at T_{irr} ~ 400 °C, and data from Patel et al. at T_{irr} ~ 500 °C [9,12,22]. Finally, there seems to be saturation of Δc/c and Δa/a values to accumulated displacement dose.

The differences between ion and neutron data have not been resolved. Briefly, there remains disagreement over (α-)Ti_3AlC_2 decomposition to TiC and lattice expansions of Δc/c and Δa/a. XRD data from Wang et al. showed the fixed position of the (008) peak at displacement doses of 4, 11 and 52 dpa; their sample did not have c-axis expansion [10]. Extensive SADP by Yang et al. noted no TiC formation, but correlated their diffraction pattern to a modified β-Ti_3AlC_2 at 31 dpa [5]. β-Ti_3AlC_2 is characterized by a change in stacking sequence as Al moves from Wyckoff 2b to 2d (center of the (004) plane), and Yang and Huang et al. added interstitial carbons to the lattice [5,11]. The "remaining" post-irradiation α-Ti_3AlC_2 showed insignificant lattice parameter expansion [11]. Regarding TiC, there remains the problem of the peak

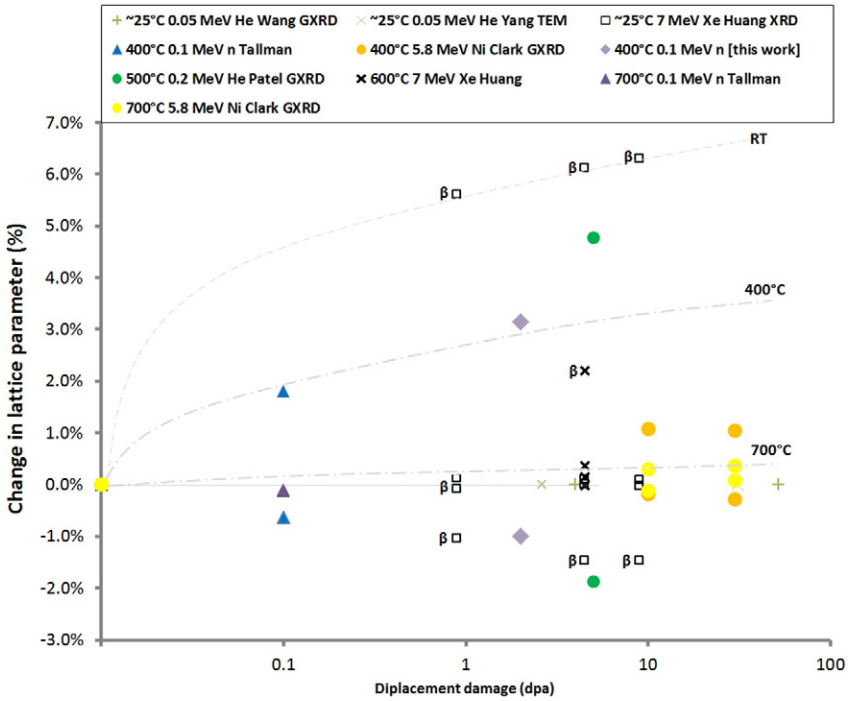

Fig. 3. The effect of radiation dose on lattice parameter changes of Ti_3AlC_2 (α-Ti_3AlC_2) compiled from current data; β indicates the "modified β-Ti_3AlC_2" suggested by Huang and Yang et al. [5,7,9–12]. Dotted curves indicate the approximate c-axis swelling and temperature relationship between 0% and 7%. Values below zero are all a-axis shrinkage.

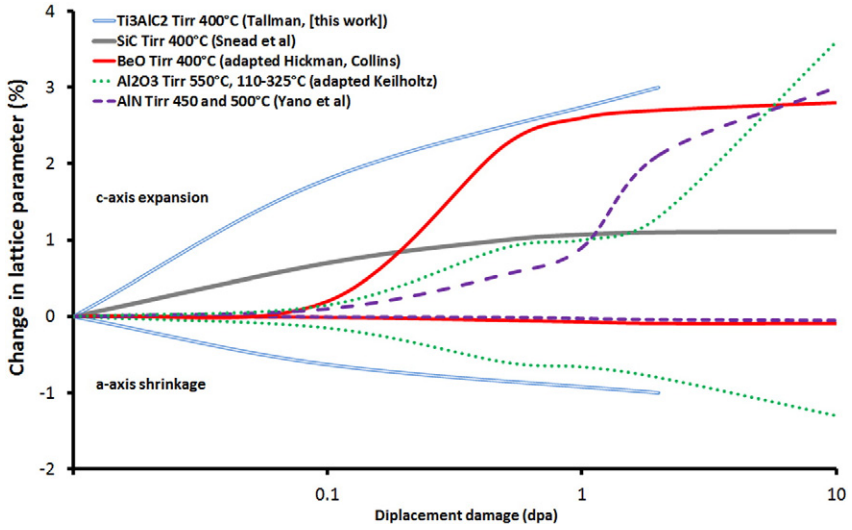

Fig. 4. Schematic trends for Δa/a and Δc/c of Ti_3AlC_2, SiC (isotropic), BeO, AlN and Al_2O_3 at similar or adapted T_{irr} from neutron irradiation data [9,19,20,23,25–32].

overlap previously discussed. Secondly, TiC is often present as an impurity. For example, ion irradiation data from Song et al. appeared to show TiC peaks (311) and (222) at 72.5° and 76° respectively in the virgin material [6]. In contrast, Wang et al. has clearly defined (111) and (200) TiC peaks from 4, 11 and 31 dpa that were absent from his virgin material (up to 2θ ~60°) [10]. In general, XRD/GXRD analysis has been hampered by the absence of the classical high angle "fingerprint" region, e.g. TiC (420) should be clear of both Ti_2AlC and Ti_3AlC_2 reflections and can be used to prove long range order and phase decomposition. Similar problems are found in SADP "fuzzy" low index reflections [10]. A sample with substantial phase segregation to verify TiC is required, such as the data reported by Tallman et al. where half of the material decomposed to TiC according to XRD analyses [9].

In Fig. 3, the data shows a tendency toward saturation of swelling from ~1–2 dpa. This is broadly comparable to SiC at T_{irr} ~ 400 °C, where the volume change attributed to unit cell expansion is about 1–2% depending on purity [23]. In SiC, point-defect swelling behavior is mitigated by increasing T_{irr} because interstitial clusters exhibit progressively reduced thermal stability [23]. Vacancy migration energies are similar to Ti_3AlC_2; V_C and V_{Si} are 3.4 and 2.4 eV in SiC, and 3.1 eV and 4.1 eV for V_{Ti1} and V_C in Ti_3AlC_2 [23,24]. These vacancies are immobile at 400 °C. In Ti_3AlC_2, migration energies for I_C in the Ti–Al plane are 0.55 eV, and I_C sites have formation energies ranging from −6.31 to −7.22 eV, indicating that I_C will play a role in defect accumulation [24]. Fig. 4 shows a schematic of both Δc/c and Δa/a values of SiC, Ti_3AlC_2, and more comparable HCP ceramics like BeO, AlN and Al_2O_3 from data at T_{irr} ~ 400 °C. The point-defect swelling behavior of SiC and Ti_3AlC_2 is similar. However, $\Delta V_{irr}/V_{irr}$ is isotropic in SiC whereas it is highly anisotropic in Ti_3AlC_2, leading to differences in grain boundary stresses and Ti_3AlC_2 microcracking.

In Al_2O_3 irradiated at T_{irr} ~ 110–325 °C, both Δa/a and Δc/c values expand with increasing dose, initially saturating until the accumulation of dislocation loops causes a preferential saturation of vacancies; at higher T_{irr}, this later leads to void swelling and microcracking once $\Delta V_{irr}/V_{irr}$ reaches ~4% [19,25,28]. In AlN, lattice parameters are highly anisotropic, with positive Δc/c values and no change in Δa/a, with onset of microcracking within ~1–2% ΔV/V [30]. In BeO, data extrapolated to T_{irr} ~ 400 °C shows c-axis expansion to ~2.5%, while the a-axis change is ~0.1% or slightly shrinks [26,27]. With BeO, as T_{irr} increases, ΔV/V notably reduced, which correlates to Ti_3AlC_2 saturation behavior [26,27]. Interestingly, BeO also has an α to β transition with a ~6% c-axis LP expansion [20].

In Fig. 3, if "modified β-Ti_3AlC_2" (marked as β) lattice parameters are included, the conflict between decomposition to β-Ti_3AlC_2 and TiC/Ti_2C_3 appears to be resolved if it is considered as strain-induced transformation [5,9,11,22]. Accumulation of point defects or larger clusters such as dislocation loops can induce crystallographic strain and a "modified β phase" bring the values for room temperature irradiation lattice swelling to consistency with other reported values. The absence of amorphization during room temperature irradiation up to ~51 dpa also indicates that irradiation below room temperature would be needed in order to stabilize sufficiently high concentrations of point defects to induce an amorphous phase transition [10]. Finally, irradiation induced swelling is mitigated at ~700 °C; Ti_3AlC_2 may be viable for use in a higher temperature regime. The neutron irradiation temperature in this work is just above the operating temperature of LWRs. The observed anisotropic swelling, pronounced cracking and poor mechanical strength indicates that Ti_3AlC_2 is unsuitable for LWR environments.

The authors would like to thank Anne Campbell, Chad Parish, Felipe Mora, Brian Eckhart, Michael McAlister, Patricia Tedder, Jordan Couch, Marie Williams, Bill Comings, Kenneth Curtis and Kurt Terrani. This research was supported by the U.S. Department of Energy, Office of Science, Fusion Energy Sciences. This manuscript has been authored by UT-Battelle, LLC, under Contract No. DE-AC05-00OR22725 with the U.S. Department of Energy. The United States Government and the publisher, by accepting the article for publication, acknowledges that the United States Government retains a non-exclusive, paid-up, irrevocable, world-wide license to publish or reproduce the published form of this manuscript, or allow others to do so, for United States Government purposes. The Department of Energy will provide public access to these results of federally sponsored research in accordance with the DOE Public Access Plan (http://energy.gov/downloads/doe-public-access-plan).

References

[1] M.W. Barsoum, Prog. Solid State Chem. 28 (2000) 201–281.
[2] M.W. Barsoum, T. El-Raghy, Am. Sci. 89 (2001) 334–343.
[3] M.W. Barsoum, T. Zhen, S.R. Kalidindi, M. Radovic, A. Murugaiah, Nat. Mater. 2 (2003) 107–111.
[4] S.J. Zinkle, L.L. Snead, Annu. Rev. Mater. Res. 44 (2014) 241–267.
[5] T. Yang, C. Wang, C.A. Taylor, X. Huang, Q. Huang, F. Li, L. Shen, X. Zhou, J. Xue, S. Yan, Y. Wang, Acta Mater. 65 (2014) 351–359.
[6] P. Song, J. Sun, Z. Wang, M. Cui, T. Shen, Y. Li, L. Pang, Y. Zhu, Q. Huang, J. Lü, Nucl. Instrum. Methods Phys. Res., Sect. B 326 (2014) 332–336.
[7] C.X. Wang, T.F. Yang, S.Y. Kong, J.R. Xiao, J.M. Xue, Q. Wang, C.F. Hu, Q. Huang, Y.G. Wang, J. Nucl. Mater. 440 (2013) 606–611.
[8] C. Liu, L. Shi, Q. Qi, D.J. O'Connor, B.V. King, E.H. Kisi, X.B. Qing, B.Y. Wang, Nucl. Instrum. Methods Phys. Res., Sect. B 307 (2013) 536–540.
[9] D.J. Tallman, E.N. Hoffman, E.a.N. Caspi, B.L. Garcia-Diaz, G. Kohse, R.L. Sindelar, M.W. Barsoum, Acta Mater. 85 (2015) 132–143.
[10] C. Wang, T. Yang, S. Kong, J. Xiao, J. Xue, Q. Wang, C. Hu, Q. Huang, Y. Wang, J. Nucl. Mater. 440 (2013) 606–611.

[11] Q. Huang, R. Liu, G. Lei, H. Huang, J. Li, S. He, D. Li, L. Yan, J. Zhou, Q. Huang, J. Nucl. Mater. 465 (2015) 640–647.
[12] Master's Thesis. D.W. Clark, M.K. Patel, C.M. Parish, S.J. Zinkle, Department of Nuclear Engineering, University of Tennessee, Pasqua Engineering Building, 2016.
[13] S.N. Votinov, V.P. Kolotushkin, S.A. Nikulin, V.Y. Turilina, Met. Sci. Heat Treat. 51 (2009) 238–244.
[14] L.L. Snead, A.M. Williams, A.L. Qualls, M.L. Grossbeck, et al., in: M.L. Grossbeck (Ed.), 21st Int. Symp. on Effects of Radiation on Materials, ASTM International, West Conshohocken, PA, 2003 (ASTM STP 1447).
[15] J.I. Bramman, A.S. Fraser, W.H. Martin, J. Nucl. Eng. 25 (1971) 223–240.
[16] Y. Katoh, A. Clark, K. Ozawa, in: B. Wiffen (Ed.), Semiannual Progress Report, Oak Ridge National Laboratory 2010, pp. 158–163.
[17] A.C. Larson, R.B.V. Dreele, Los Alamos National Laboratory Report LAUR 86, 2000.
[18] S. Kondo, Y. Katoh, L.L. Snead, J. Nucl. Mater. 417 (2011) 406–410.
[19] T.M. Sabine, J. Nucl. Mater. 33 (1969) 340–342.
[20] R.S. Wilks, J. Nucl. Mater. 26 (1968) 137–173.
[21] T. Yano, T. Iseki, J. Nucl. Mater. 179–181 (1991) 387–390 Part 1.
[22] M.K. Patel, D.J. Tallman, J.A. Valdez, J. Aguiar, O. Anderoglu, M. Tang, J. Griggs, E.G. Fu, Y.Q. Wang, M.W. Barsoum, Scr. Mater. 77 (2014) 1–4.
[23] L.L. Snead, T. Nozawa, Y. Katoh, T.-S. Byun, S. Kondo, D.A. Petti, J. Nucl. Mater. 371 (2007) 329–377.
[24] S.C. Middleburgh, G.R. Lumpkin, D. Riley, J. Am. Ceram. Soc. 96 (2013) 3196–3201.
[25] F.W. Clinard Jr., G.F. Hurley, L.W. Hobbs, J. Nucl. Mater. 108–109 (1982) 655–670.
[26] C.G. Collins, J. Nucl. Mater. 14 (1964) 69–86.
[27] B.S. Hickman, W.B. Rotsey, K. Veevers, J. Nucl. Mater. 20 (1966) 122–125.
[28] B.S. Hickman, D.G. Walker, J. Nucl. Mater. 18 (1966) 197–205.
[29] G.W. Keilholtz, R.E. Moore, H.E. Robertson, Nucl. Technol. 17 (1973) 234–246.
[30] T. Yano, T. Iseki, J. Nucl. Mater. 203 (1993) 249–254.
[31] Y. Katoh, L.L. Snead, I. Szlufarska, W.J. Weber, Curr. Opin. Solid State Mater. Sci. 16 (2012) 143–152.
[32] Y. Katoh, L.L. Snead, C.H. Henager Jr., T. Nozawa, T. Hinoki, A. Iveković, S. Novak, S.M. Gonzalez de Vicente, J. Nucl. Mater. 455 (2014) 387–397.